



Search for a Fermiophobic Higgs Boson in the Di-photon Final State Using 10 fb^{-1} of CDF Data

The CDF Collaboration
URL <http://www-cdf.fnal.gov>
(Dated: July 26, 2012)

A search for a fermiophobic Higgs boson in the di-photon final states is reported based on CDF data from 10 fb^{-1} of integrated luminosity from $p\bar{p}$ collisions at $\sqrt{s}=1.96 \text{ TeV}$. We improve upon the previous CDF result by adding 43% of more data. In contrast with the Standard Model, the coupling of the Higgs boson to fermions is suppressed in fermiophobic models. Therefore, the diphoton decay mode can be greatly enhanced. In the presented note, no evidence of a resonance in the diphoton spectrum is observed, and upper limits are set on the cross section times branching fraction of the resonant state as a function of Higgs boson mass. We found an observed (expected) limit on the fermiophobic Higgs boson production excluding Higgs bosons particles with a mass $m_{h,f} < 114 \text{ GeV}/c^2$ ($m_{h,f} < 113 \text{ GeV}/c^2$) at the 95% confidence level.

Preliminary Results

I. INTRODUCTION

The Standard Model (SM) prediction for $\gamma\gamma$ branching fraction is extremely small. However, in “fermiophobic” models, the coupling of the Higgs boson to fermions is suppressed. Thus, the decay of the Higgs boson to diphoton is greatly enhanced. In the SM, the spontaneously symmetry breaking mechanism requires a single doublet of a complex scalar field. However, nature does not have to follow this minimal version and that may require a multi-Higgs sector. Thus, extended Higgs sectors with doublets and triplets fields are in the market [1] [2]. We consider in this note a model that requires a doublet field. In this model, it is possible that the symmetry breaking mechanism responsible for giving masses to gauge bosons is separate from that which generates the fermion masses.

An informative summary of the various models that modify $B(h \rightarrow \gamma\gamma)$ can be found in Reference [3]. The “fermiophobic” Higgs (h_f) benchmark model assumes SM coupling to bosons and vanishing couplings to all fermions. In the case of h_f , gluon-fusion production vanishes and only associated production with a W or Z boson and vector boson fusion (VBF) remain. This results in a reduction in the production cross section by about a factor of four; however, this reduction is compensated by the branching fraction for these models, which can be larger by more than two orders of magnitude for low mass Higgs. For example, the branching fraction has as a value of one order of magnitude higher than those at SM for Higgs masses of about 120 GeV/ c^2 . The higher branching fraction causes a larger number of potential fermiophobic Higgs events compared to SM Higgs.

The diphoton final state is also appealing for a Higgs boson search because the photon ID efficiency and energy resolution are better than that of jets. The photons better energy resolution leads to a narrow mass peak which can be exploited to reduce background.

In the past, there have been phenomenological discussions of searches for h_f at the Tevatron experiments [4], as well as experimental searches at LEP [5]. In Run I, CDF searched for the fermiophobic Higgs [6] and recently for Run II, DØ published a paper [7] focusing on the same search. Moreover, CDF published a search for h_f with $\sim 3 \text{ fb}^{-1}$ [8] and DØ published a search for the SM Higgs with $\sim 2.7 \text{ fb}^{-1}$ [9]. Most recently, CDF published a search for SM and Fermiophobic Higgs models with $\sim 7 \text{ fb}^{-1}$ [10] and DØ published a search for a similar search using $\sim 8.2 \text{ fb}^{-1}$ of data [11]. The ATLAS and CMS experiments at CERN furthermore have preliminary results in the $\gamma\gamma$ decay mode that exclude fermiophobic Higgs masses in the range 110.0–124.5 GeV/ c^2 and 127–137.5 GeV/ c^2 [12, 13].

In this note, we report the sensitivity of a CDF search for fermiophobic $H \rightarrow \gamma\gamma$. We update the most recent 7.0 fb^{-1} analysis in this channel [14] with the incorporation of the final dataset taken up to the Tevatron shutdown in September, 2011. Diphoton events are divided into four independent subsamples according the position and type of the photon candidate. In CC events (the most sensitive category), there are two photons in the central region of the detector. In CP events, one photon is in the central region and one is the plug region. For each of these categories, the two highest p_T photons in the sample are selected. If a CC or CP event is not identified, then two additional categories are considered. In C’C events, both photons are central but one has converted and is reconstructed from its e^+e^- decay products. Finally, in C’P events, one photon is in the plug region and the other is a central conversion photon.

In order to improve sensitivity, the event selection was further extended to take advantage of the final state features present in these production modes. Associated production dominates the production process, so the optimization was carried out on the basis of the associated production process alone. A selection based on the fact that fermiophobic Higgs events will be produced with Z or W bosons or two jets which will balance the high diphoton transverse momentum $p_T^{\gamma\gamma}$. We considered the cut of 75 GeV as in the previous analysis which is termed as the high $p_T^{\gamma\gamma}$ bin. Moreover, we added two more p_T bins, $35 \text{ GeV} < p_T^{\gamma\gamma} < 75 \text{ GeV}$ (medium $p_T^{\gamma\gamma}$ bin) and $p_T^{\gamma\gamma} < 35 \text{ GeV}$ (low $p_T^{\gamma\gamma}$ bin).

All cross sections are calculated by HIGLU and branching fractions are calculated by HDECAY [15]. These values are summarized in Table I.

II. THE CDF DETECTOR

A detailed description of the CDF detector is described in many available references [16, 17].

III. DATA SETS AND GLOBAL EVENT SELECTION

This analysis uses data from February 2004 through September 2011, comprising 10.0 fb^{-1} of integrated luminosity for the CC category, and 9.34, 9.87, and 9.28 fb^{-1} for the CP, C’C, and C’P categories, respectively. Signal Monte Carlo (MC) was generated using PYTHIA 6.2 [18], CTEQ5 [19] parton distribution functions, and the standard CDF underlying event tune [20]. Samples for masses between 100 – 150 GeV/ c^2 in 5 GeV/ c^2 intervals were developed and used.

M_h (GeV/ c^2)	$\sigma(Wh)$ pb	$\sigma(Zh)$ pb	$\sigma(VBF)$ pb	$B(h_f \rightarrow \gamma\gamma)$
100	0.2811	0.1627	0.0973	0.185
105	0.2387	0.1395	0.0898	0.104
110	0.2037	0.1202	0.0828	0.0603
115	0.1745	0.1039	0.0765	0.0366
120	0.1501	0.0902	0.0707	0.0233
125	0.1295	0.0785	0.0653	0.0156
130	0.1120	0.0685	0.0605	0.0107
135	0.0972	0.0600	0.0560	0.0075
140	0.0846	0.0527	0.0519	0.0054
145	0.0737	0.0463	0.0480	0.0039
150	0.0644	0.0408	0.0445	0.0027

TABLE I: Cross section for Fermiophobic Higgs production, and its branching fractions decay to diphotons for many mass points.

The events are selected by a three-level trigger system that requires an isolated cluster of energy deposited in the EM calorimeter with a transverse energy $E_T > 25$ GeV [30]. The trigger efficiency for events that pass the full diphoton selection is essentially 100% for the most sensitive event category (CC) and above 90% for all other categories. The global event selection then requires that the data included in the analysis was taken during good detector conditions. The reconstructed event vertex is determined from the vertex with highest sum p_T of the associated tracks, and the z position of this vertex must be within 60 cm of zero. The overall efficiency for this cut, measured from the data, is $97.43 \pm 0.07\%$.

IV. PHOTON IDENTIFICATION

The dominant backgrounds to prompt photons originating from the event vertex are electrons faking photons and jets faking photons. The latter is more frequent and typically occurs when a jet fragments into a π^0 or η meson which then decays to multiple photons. These delayed photons are collinear and are often mis-reconstructed as a single photon. A set of photon selection requirements are then applied in order to identify high-energy prompt photons with $p_T > 15$ GeV/ c , and to reduce these backgrounds.

A. Central Photon ID

A neural network (NN) technique is used to identify photons in the central region of the detector ($|\eta| < 1.05$). Central photon candidates are first required to satisfy loose selection requirements as described in Ref. [21]. After additional track requirements are applied to remove electrons, the remaining candidates are required to have a NN output value above a threshold that is selected to maximize a $H \rightarrow \gamma\gamma$ signal to background figure of merit. As more than half of the events in the data with two photon candidates contain either one or two jets misidentified as a prompt photon, the NN discriminant is trained using photon and jet Monte Carlo (MC) samples and constructed from several detector variables that distinguish true photons from these jet backgrounds. These variables also allow the NN method to be applied to electrons, which are used to calibrate ID efficiencies. These variables include the ratio of energy in the shower maximum detector to that in the calorimeter cluster associated with the photon, the ratio of hadronic to EM transverse energy (Had/EM), calorimeter and track isolation [21], and a χ^2 value calculated by comparing the measured transverse shower profile to that of a single EM shower [22].

This NN method increases the photon signal efficiency by $\sim 5\%$ and background rejection by $\sim 12\%$ compared to the standard selection requirements for central photons [21], which improves $H \rightarrow \gamma\gamma$ sensitivity by about 9%. Signal efficiency is calculated using $Z \rightarrow e^+e^-$ events in both the data and MC, as a function of the number of vertices (N_{vtx}) in the event. Net efficiencies for the data and simulation are obtained by taking the weighted average of the efficiencies over the number of vertices in the diphoton sample and Higgs signal MC. A data-MC scale factor is then determined based on the difference in the signal efficiency as measured from the data relative to that predicted by the MC. This correction factor is included when normalizing the Higgs signal mass shape.

Several sources of systematic uncertainty were considered. Photon ID efficiencies are studied using electrons from Z boson decays; however, there are small differences in the shower profiles of electrons and photons which may affect these studies. To account for this, a systematic of 1% was taken based on the difference between photon and

electron ID efficiencies observed in the MC with detector simulation. For this comparison, $\gamma \rightarrow e^+e^-$ conversions were removed from the photon MC which are not in the Z MC. An uncertainty of 0.2% on the efficiency of removing these conversions is applied and is due to the uncertainty in the material included in the simulation of the CDF detector. A single data-MC scale factor is applied to the full MC sample; however, the variations of this factor between data taking periods was included as a systematic of 1.5%. Finally, the uncertainties on the Z boson mass fits in data and MC used to study ID efficiencies are propagated as an uncertainty of 0.2%.

B. Plug Photon ID

We include photons with $1.2 < |\eta| < 2.8$ using standard CDF photon ID [21] based on similar variables described for central photons: the ratio of energy in the shower maximum detector to that in the calorimeter cluster associated with the photon, the ratio of hadronic to EM transverse energy (Had/EM), calorimeter and track isolation [21], and a χ^2 value calculated by comparing the measured transverse shower profile to that of a single EM shower [22]. Data-MC scale factors are obtained and applied to the normalization of the Higgs signal mass shape using the same techniques as for central photons. The same sources of systematic uncertainty on photon ID for central photons are applied to plug photons. Uncertainty from the difference between electron vs photon ID is taken to be 2.6%, from detector material to be 3.0%, from data taking periods to be 2.0%, and from data/MC fits of the Z mass to be 0.8%.

C. Central Conversion Photon ID

As photons pass through detector material, electromagnetic interactions with a nucleus can cause photons to convert into an electron-positron pair. Using photon MC truth information it was found that this occurs approximately 15% of the time in the central region of the detector, so for the CC channel about 26% of events are lost (where we ignore double conversion events) and about 15% of events are lost in the CP channel. Due to lower tracking efficiency in the plug region we only consider central conversion photons.

In order to recover central conversion photons, we search for an electron with $|\eta| < 1.05$ (the “primary” and higher E_T leg) with a nearby track corresponding to a particle of opposite charge and with a minimum $p_T = 1.0$ GeV/c (the “secondary” leg). The proximity of the two particle tracks is first determined by requiring the transverse distance between the two tracks to be less than 0.2 cm at the radial location where they are parallel. The difference in $\cot \theta$ between the two tracks must be less than 0.04, where $\cot \theta = p_z/p_T$. Backgrounds are further removed by allowing only a small fraction of hadronic E_T associated with the primary electron’s cluster. Additionally, requirements are made on the conversion candidate’s calorimeter isolation. This quantity is obtained from the primary electron’s calorimeter isolation [21], with the secondary electron’s p_T subtracted if its track points to a different calorimeter ϕ tower. The ratio of transverse energy to transverse momentum (E/p) shape is peaked at one for isolated photon conversions, but has a long tail for photon conversions from π^0 or $\eta \rightarrow \gamma\gamma$ decays due to the extra energy from the unconverted photon. Restrictions on this ratio then further remove jet backgrounds. The conversion E_T is obtained from the primary electron’s E_T with the secondary electron’s p_T added if it is in a different calorimeter tower while the photon’s reconstructed transverse momentum is obtained by adding the vector sum of the two track’s momenta at the radius of the conversion.

The direction of the conversion photon’s momentum is obtained by taking the vector sum of the individual track momenta; however, better $H \rightarrow \gamma\gamma$ mass resolution is obtained by setting the total momentum to be the conversion’s energy obtained from EM calorimeters, which additionally constrains the photon’s mass to zero.

An uncertainty on this selection is obtained using $Z \rightarrow e^\pm +$ trident events in the data and MC, where a trident is defined as an electron that radiates a photon via bremsstrahlung which then converts to an electron-positron pair ($e^\mp \gamma \rightarrow e^\mp e^+ e^-$). Due to the lower energy range of the conversion photons of this method compared to those from $H \rightarrow \gamma\gamma$, it was chosen not to apply a data-MC scale factor to simulated events but instead to use the difference in the calculated scale factor from one to obtain an uncertainty on conversion ID. This was estimated by comparing the ratio of number of trident events selected to the number of regular $Z \rightarrow e^+e^-$ events selected in both the data and MC. This ratio was chosen in order to remove dependence on uncertainties from sources such as trigger efficiency, luminosity, and Z cross section. The result gives a 7% uncertainty which is applied as a systematic on conversion ID.

V. DETECTOR ACCEPTANCE

The detector acceptance was studied using PYTHIA Monte Carlo production events passed through a simulation for the CDF detector, CDFSIM, based on GEANT [23] and GFLASH [24]. The remaining events that additionally passed the

same photon ID selection as the data, were then used to obtain an overall signal acceptance for each signal process and mass point. These values are multiplied by the z vertex efficiency, the trigger efficiency, and the data-MC correction factors to obtain acceptance times efficiency values (ϵA) for each Higgs boson test hypothesis, diphoton category, and production method. An example of these values is provided in Section VIII.

VI. SYSTEMATIC UNCERTAINTIES ON SIGNAL

Systematic uncertainties on signal MC are summarized in Table II and include uncertainties in the production cross section, the integrated luminosity, and on the acceptance and efficiency. A 6% uncertainty on the integrated luminosity considers uncertainty in $p\bar{p}$ inelastic cross section and acceptance of CDF's luminosity monitor. The theoretical uncertainties on the production cross sections used are 7% for associative Higgs production with a W or Z , and 5% for vector boson fusion. All systematics on ID efficiency for photons were described in section IV.

The PDF uncertainty on event acceptance was calculated using the CTEQ61.M [25, 26] error sets and a standard event re-weighting technique [27, 28]. Initial and final state radiation (ISR and FSR) uncertainties were studied using MC samples with modified parton shower parameters and we correlate them. The energy scale systematic uncertainty of the central/plug electromagnetic calorimeters (CEM/PEM) was studied by checking the effect on the acceptance of varying the CEM/PEM scale by 1% to obtain 0.1% for central and 0.8% for plug.

The z vertex uncertainty is based on the uncertainty in the $|z| < 60$ cm requirement described in Section III. The trigger efficiency uncertainty is based on differences in the efficiency predicted from the MC compared with that from the data.

The uncertainty on PYTHIA modeling of the shape of the $p_T^{\gamma\gamma}$ distribution for the signal was estimated to be (4%) for the high p_T bin and (2%) for the medium and low p_T bins. The latter uncertainty was estimated by studying the effect on the acceptance from the differences in the shape of the p_T distribution from leading-order, next-to-leading order, Collins-Soper-Sterman (CSS) and PYTHIA predictions [29].

CDF Run II Preliminary	$\int \mathcal{L} = 10.0 \text{ fb}^{-1}$			
	Systematic Errors on Signal (%)			
	CC	CP	C'C	C'P
Luminosity	6	6	6	6
σ_{VH}	7	7	7	7
σ_{VBF}	5	5	5	5
PDF	2	2	2	2
ISR/FSR	5	6	8	6
Energy Scale	0.2	0.8	0.1	0.8
Trigger Efficiency (high p_T)	1	1.3	1	1
Trigger Efficiency (medium p_T)	1	1.3	1	7
Trigger Efficiency (low p_T)	1	1.3	2	9
Z Vertex	0.2	0.2	0.2	0.2
Conversion ID	–	–	7	7
Material Uncertainty	0.4	3.0	0.2	3.0
Photon/Electron ID	1.0	2.8	1.0	2.6
Run Dependence	3.0	2.5	1.5	2.0
Data/MC fits	0.4	0.8	1.5	2.0
$p_T^{\gamma\gamma}$ PYTHIA/NLO	4	4	4	4

TABLE II: Summary of systematic errors applied to signal.

VII. BACKGROUND MODEL

The width of the $M_{\gamma\gamma}$ signal peak is on the order of a few GeV/c^2 and is mostly limited by detector resolution. This means that we are searching for a very narrow peak on a smooth background distribution (Figures 1, 2) composed of both SM diphoton events and events in which one or two jets fake a photon. For regular photons, this smooth region of the data is composed of both SM diphoton events and events in which one or two jets fake a photon. For conversion photons, this region of the data is mostly composed of real conversions from jets and jets faking a conversion photon. Modeling of the background combinations is possible, but non-trivial, and is not necessary for

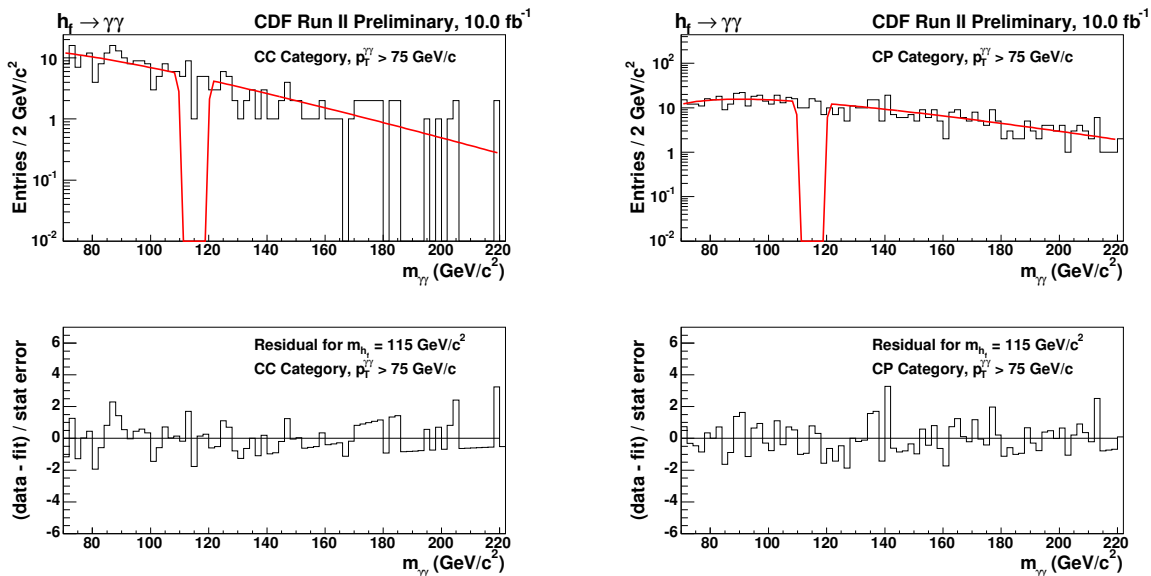


FIG. 1: Smooth fits to the signal region in the data for CC channel (left) and CP channel (right) with the fermiophobic Higgs event selection for the high $p_T^{\gamma\gamma}$ bin. The example fit shown was obtained by first excluding a $12 \text{ GeV}/c^2$ window around a signal mass of $M_h = 115 \text{ GeV}/c^2$ and then interpolating into this region. The fit in the signal region will serve as the null hypothesis background model. The data-fit residuals are also shown.

dedicated searches for a narrow mass peak. Therefore, rather than model each background component directly, a null hypothesis is assumed after visual confirmation that no significant peak exists in the data, a smooth curve is fit to the data. This fit excludes a signal window around each mass point and is then interpolated into the signal region. The mass window is $12 \text{ GeV}/c^2$ for $M_h = 100\text{--}115 \text{ GeV}/c^2$, $16 \text{ GeV}/c^2$ for $M_h = 120\text{--}135 \text{ GeV}/c^2$, and $20 \text{ GeV}/c^2$ for $M_h = 140\text{--}150 \text{ GeV}/c^2$. The fit in the signal region serves as the background model for predicting the expected sensitivity and for testing against the data for the signal hypotheses at the various mass points.

In this analysis, we considered three $p_T^{\gamma\gamma}$ bins. For the high and medium $p_T^{\gamma\gamma}$ bins, the statistics were low and we used a fitting function with only four parameters. For the lower $p_T^{\gamma\gamma}$ bin, the statistics were high and we used a function with six parameter. One modification to this method is made for the CP channels that are contaminated by a large contribution of $Z \rightarrow e^+e^-$ backgrounds which is visible as a peak in the data. The Z background could be modeled by MC and added then to the smooth portion, but we can also more simply further our current method by adding an appropriate function to describe the peak made by the Z boson. It was found that a Breit-Wigner function well describes this region of the $M_{\gamma\gamma}$ distribution for the CP channels, so it was added to the smooth function used to fit to the rest of the data.

An example fit for each channel, obtained from a mass window around $115 \text{ GeV}/c^2$, is shown in Figures 1 – 2, along with the corresponding residual plot of $(\text{data} - \text{fit})/(\text{stat error})$. The stability of the fits in the signal region used for setting limits was studied by fluctuating the parameter values of the fit and then taking the average of the smallest and largest integral differences from that of the standard function. In general, these values reflect the statistics in the respective mass distributions as higher statistics constrains the amount by which the fit will fluctuate as parameter values are varied. The results were used to obtain a background rate uncertainties for each channel and mass are about 10.5%, 5.7%, 17.2%, and 17.3% applied to the CC, CP, CC conversion, and CP conversion channels respectively in the case of high $p_T^{\gamma\gamma}$ bin. For the medium $p_T^{\gamma\gamma}$ bin, we found that the background rate uncertainties for each channel and mass are about 8.3%, 2.5%, 12.1%, and 8.8% applied to the CC, CP, CC conversion, and CP conversion channels respectively. Finally, we found that the background rate uncertainties for each channel and mass are about 3.5%, 1.3%, 7.1%, and 2.9% applied to the CC, CP, CC conversion, and CP conversion channels respectively for the low $p_T^{\gamma\gamma}$ bin. Cross checks on these values were done by either replacing or modifying the fit function. From these studies, variations of the test background yields in the signal regions as compared to that of the standard were consistent with uncertainties already obtained.

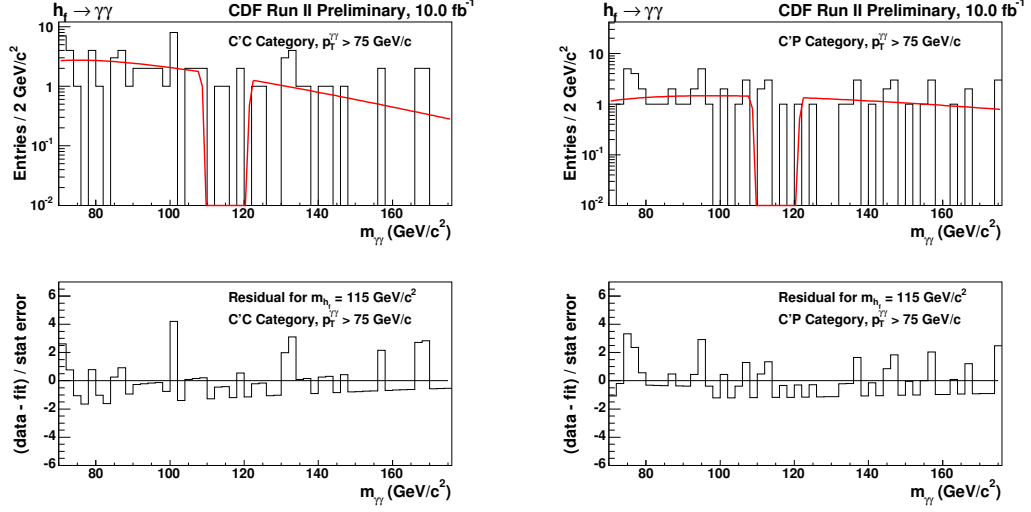


FIG. 2: Smooth fits to the signal region in the data for CC conversion channel (left) and CP conversion channel (right) with the fermiophobic Higgs event selection for the high $p_T^{\gamma\gamma}$ bin. The example fit shown was obtained by first excluding a $12 \text{ GeV}/c^2$ window around a signal mass of $M_h = 115 \text{ GeV}/c^2$ and then interpolating into this region. The fit in the signal region will serve as the null hypothesis background model. The data-fit residuals are also shown.

VIII. RESULTS

We set upper limits on production cross sections times branching ratio and the branching ratio for a fermiophobic Higgs. We calculate a Bayesian C.L. limit for each mass hypothesis based on the combined binned likelihood of the mass distributions for each channel. The results of the limit calculation are included in Table III and displayed graphically in Figure 3. The SM cross sections assumed in the benchmark fermiophobic model are used to convert the limits on $\sigma \times Br(h \rightarrow \gamma\gamma)$ into limits on $Br(h \rightarrow \gamma\gamma)$. The result sets an observed (expected) limit on the fermiophobic Higgs boson production excluding Higgs bosons particles with a mass $m_{h_f} > 114 \text{ GeV}/c^2$ ($m_{h_f} > 113 \text{ GeV}/c^2$) at the 95% confidence level.

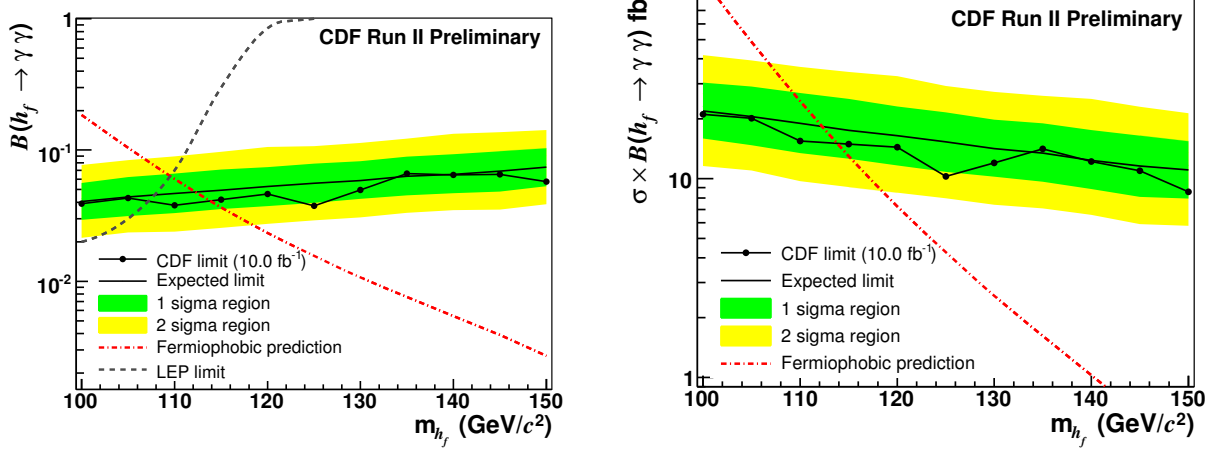


FIG. 3: The 95% C.L. upper limit on the branching fraction for the fermiophobic Higgs boson decay to diphotons, as a function of m_h (left). Similarly for the branching ratio times cross section (right).

CDF Run II Preliminary				$\int \mathcal{L} = 10.0 \text{ fb}^{-1}$		
m_h (GeV/c ²)	$\sigma \times Br(h \rightarrow \gamma\gamma)$ Limits (fb)			$Br(h \rightarrow \gamma\gamma)$ Limits (%)		
	Expected	Observed	Model expectation	Expected	Observed	Model expectation
100	21.88	21.07	100.10	4.04	3.89	18.5
105	20.5	20.12	48.67	4.38	4.29	10.4
110	18.98	15.44	24.52	4.66	3.79	6.03
115	17.51	14.89	12.98	4.93	4.19	3.66
120	16.44	14.37	7.24	5.28	4.62	2.33
125	15.29	10.25	4.26	5.59	3.75	1.56
130	14.14	11.98	2.57	5.86	4.97	1.07
135	13.45	14.12	1.61	6.30	6.62	0.759
140	12.36	12.2	1.02	6.53	6.44	0.544
145	11.58	10.94	0.65	6.89	6.51	0.39
150	11.07	8.59	0.40	7.39	5.73	0.27

TABLE III: Observed and expected 95% C.L. limits on the production cross section and branching fraction and theory predictions for the fermiophobic benchmark Higgs boson model.

IX. CONCLUSIONS

We presented the results of a search for a narrow resonance in the diphoton mass spectrum using 10.0 fb⁻¹ of data taken by the CDF II detector at the Tevatron. There is no evidence of a narrow resonance. Limits are placed on the production cross section and the branching fraction for the Higgs boson decay into a photon pair and compared to the predictions of a benchmark fermiophobic model. We found an observed (expected) limit on the fermiophobic Higgs boson production excluding Higgs bosons particles with a mass $m_{h_f} < 114 \text{ GeV}/c^2$ ($m_{h_f} < 113 \text{ GeV}/c^2$) at the 95% confidence level.

Acknowledgments

We thank the Fermilab staff and the technical staffs of the participating institutions for their vital contributions. This work was supported by the U.S. Department of Energy and National Science Foundation; the Italian Istituto Nazionale di Fisica Nucleare; the Ministry of Education, Culture, Sports, Science and Technology of Japan; the Natural Sciences and Engineering Research Council of Canada; the National Science Council of the Republic of China; the Swiss National Science Foundation; the A.P. Sloan Foundation; the Bundesministerium fuer Bildung und Forschung, Germany; the Korean Science and Engineering Foundation and the Korean Research Foundation; the Particle Physics and Astronomy Research Council and the Royal Society, UK; the Russian Foundation for Basic Research; the Comision Interministerial de Ciencia y Tecnologia, Spain; and in part by the European Community's Human Potential Programme under contract HPRN-CT-20002, and the Academy of Finland.

-
- [1] A. Barroso, L. Brucher, and R. Santos, Phys. Rev. **D60**, 035005 (1999), hep-ph/9901293.
 - [2] J. Gunion, R. Vega, and J. Wudka, Phys. Rev. **D42**, 1673 (1990).
 - [3] S. Mrenna and J. D. Wells, Phys. Rev. **D63**, 015006 (2001), hep-ph/0001226.
 - [4] G. L. Landsberg and K. T. Matchev, Phys. Rev. **D62**, 035004 (2000), hep-ex/0001007.
 - [5] L. Authors (LEP Higgs Working Group) (2001), hep-ex/0107035.
 - [6] A. A. Affolder et al. (CDF), Phys. Rev. **D64**, 092002 (2001), hep-ex/0105066.
 - [7] V. Abazov et al. (D0) (2008), arXiv:0803.1514 [hep-ex].
 - [8] T. Aaltonen et al. (CDF), Phys. Rev. Lett. **103**, 061803 (2009), 0905.0413.
 - [9] V. Abazov et al. (D0), Phys. Rev. Lett. **102**, 231801 (2009).
 - [10] T. Aaltonen et al. (CDF) (2011), arXiv:1109.4427v2.
 - [11] V. Abazov et al. (D0), Phys. Rev. Lett. **107**, 51801 (2011).
 - [12] A. Collaboration et al. (ATLAS Collaboration) (2012), 1205.0701.
 - [13] S. Chatrchyan et al. (CMS Collaboration) (2012), 1207.1130.
 - [14] T. Aaltonen et al. (CDF Collaboration) (2011), 1109.4427.
 - [15] M. Spira (1998), hep-ph/9810289.
 - [16] F. Abe et al. (CDF), Nucl. Instr. Meth. **A271**, 387 (1988).

- [17] P. T. Lukens (CDF IIB) (2003), FERMILAB-TM-2198.
- [18] T. Sjostrand et al., Comput. Phys. Commun. **135**, 238 (2001), hep-ph/0010017.
- [19] H. L. Lai et al. (CTEQ), Eur. Phys. J. **C12**, 375 (2000), hep-ph/9903282.
- [20] R. Field and R. C. Group (CDF) (2005), hep-ph/0510198.
- [21] T. Aaltonen et al. (CDF Collaboration), Phys. Rev. D **82**, 052005 (2010).
- [22] F. Abe et al. (CDF Collaboration), Phys. Rev. D **48**, 2998 (1993).
- [23] R. Brun, F. Bruyant, M. Maire, A. C. McPherson, and P. Zancarini (1987), CERN-DD/EE/84-1.
- [24] G. Grindhammer, M. Rudowicz, and S. Peters, Nucl. Instrum. Meth. **A290**, 469 (1990).
- [25] D. Stump et al., JHEP **10**, 046 (2003), hep-ph/0303013.
- [26] J. Pumplin et al., Phys. Rev. **D65**, 014013 (2002), hep-ph/0101032.
- [27] P. M. Nadolsky and Z. Sullivan, eConf **C010630**, P510 (2001), hep-ph/0110378.
- [28] D. Bourilkov, R. C. Group, and M. R. Whalley (2006), hep-ph/0605240.
- [29] S. Mrenna and C. P. Yuan, Phys. Lett. **B416**, 200 (1998), hep-ph/9703224.
- [30] The transverse energy E_T and transverse momentum p_T are defined as $E \sin \theta$ and $|\vec{p}| \sin \theta$, respectively.

Appendix A: Event Yields and Signal Acceptances

a. $p_T^{\gamma\gamma} > 75 \text{ GeV}/c$ Region

TABLE IV: The $p_T^{\gamma\gamma} > 75 \text{ GeV}/c$ region is shown here, which provides the greatest sensitivity for a fermiophobic Higgs boson observation. For each h_f mass hypotheses tested in this analysis, the efficiency multiplied by signal acceptance (ϵA) is shown as a percentage of the total number of $h \rightarrow \gamma\gamma$ decays for each production mechanism (VH and VBF). These values, along with the cross sections and branching ratios provided in Table I, are used to obtain the predicted number of SM Higgs boson signal events. Integrated luminosities for each channel are given in Section III and provided in each subtable. The number of background and data events are also given for each mass. The final column in each subtable is the number of signal events divided by the square root of the number of background events (S/\sqrt{B}). The event yields for each mass point are obtained from a signal region centered on the Higgs boson mass hypothesis.

(a)							(b)						
Fermiophobic $h \rightarrow \gamma\gamma$				CDF Run II Preliminary			Fermiophobic $h \rightarrow \gamma\gamma$				CDF Run II Preliminary		
CC Category (10 fb^{-1})				$p_T^{\gamma\gamma} > 75 \text{ GeV}/c$			CP Category (9.3 fb^{-1})				$p_T^{\gamma\gamma} > 75 \text{ GeV}/c$		
m_h (GeV/c^2)	ϵA (%)		Event Yields				m_h (GeV/c^2)	ϵA (%)		Event Yields			
	VH	VBF	Signal	Background	Data	S/\sqrt{B}		VH	VBF	Signal	Background	Data	S/\sqrt{B}
100	4.18	4.07	41.7	41.9	42	6.4	100	3.16	2.95	29.2	85.9	95	3.2
105	4.37	4.13	21.1	39.6	36	3.4	105	3.33	3.07	14.9	83.8	91	1.6
110	4.62	4.18	11.1	32.7	35	2.0	110	3.58	3.30	8.1	81.0	82	0.9
115	4.75	4.22	6.0	30.2	31	1.1	115	3.93	3.35	4.6	79.8	73	0.5
120	5.01	4.34	3.5	34.2	37	0.6	120	4.26	3.62	2.8	103.2	79	0.3
125	5.21	4.38	2.1	32.5	30	0.4	125	4.46	3.68	1.7	98.5	74	0.2
130	5.40	4.46	1.3	28.6	23	0.3	130	4.63	3.79	1.1	85.2	83	0.1
135	5.51	4.48	0.8	26.6	18	0.2	135	4.89	3.88	0.7	76.2	90	0.08
140	5.86	4.60	0.6	28.2	20	0.1	140	5.19	3.96	0.5	88.6	100	0.05
145	5.94	4.63	0.4	24.8	20	0.07	145	5.36	4.05	0.3	84.6	94	0.03
150	6.08	4.71	0.2	21.1	17	0.05	150	5.48	4.09	0.2	77.0	79	0.02

(c)							(d)						
Fermiophobic $h \rightarrow \gamma\gamma$				CDF Run II Preliminary			Fermiophobic $h \rightarrow \gamma\gamma$				CDF Run II Preliminary		
C'C Category (9.9 fb^{-1})				$p_T^{\gamma\gamma} > 75 \text{ GeV}/c$			C'P Category (9.3 fb^{-1})				$p_T^{\gamma\gamma} > 75 \text{ GeV}/c$		
m_h (GeV/c^2)	ϵA (%)		Event Yields				m_h (GeV/c^2)	ϵA (%)		Event Yields			
	VH	VBF	Signal	Background	Data	S/\sqrt{B}		VH	VBF	Signal	Background	Data	S/\sqrt{B}
100	0.94	0.92	9.26	10	15	2.86	100	0.30	0.30	2.81	8	9	0.97
105	0.94	0.93	4.49	9	15	1.48	105	0.35	0.33	1.55	9	6	0.52
110	1.05	0.96	2.50	10	8	0.80	110	0.39	0.35	0.87	8	9	0.31
115	1.06	0.99	1.34	9	6	0.44	115	0.38	0.35	0.45	8	6	0.16
120	1.19	1.02	0.83	11	6	0.25	120	0.47	0.38	0.30	12	6	0.09
125	1.22	1.03	0.49	9	7	0.16	125	0.48	0.38	0.18	12	3	0.05
130	1.24	1.04	0.30	7	11	0.11	130	0.49	0.41	0.11	11	6	0.03
135	1.26	1.05	0.19	6	10	0.08	135	0.54	0.42	0.08	10	6	0.02
140	1.33	1.07	0.13	7	12	0.05	140	0.54	0.45	0.05	11	11	0.01
145	1.37	1.06	0.08	7	5	0.03	145	0.57	0.44	0.03	11	11	0.01
150	1.37	1.14	0.05	6	5	0.02	150	0.61	0.46	0.02	10	11	0.01

b. $35 < p_T^{\gamma\gamma} < 75 \text{ GeV}/c$ Region

TABLE V: The $35 < p_T^{\gamma\gamma} < 75 \text{ GeV}/c$ region is shown here. For each h_f mass hypotheses tested in this analysis, the efficiency multiplied by signal acceptance (ϵA) is shown as a percentage of the total number of $h \rightarrow \gamma\gamma$ decays for each production mechanism (VH and VBF). These values, along with the cross sections and branching ratios provided in Table I, are used to obtain the predicted number of SM Higgs boson signal events. Integrated luminosities for each channel are given in Section III and provided in each subtable. The number of background and data events are also given for each mass. The final column in each subtable is the number of signal events divided by the square root of the number of background events (S/\sqrt{B}). The event yields for each mass point are obtained from a signal region centered on the Higgs boson mass hypothesis.

(a)

Fermiophobic $h \rightarrow \gamma\gamma$		CDF Run II Preliminary				
CC Category (10 fb^{-1})		$35 < p_T^{\gamma\gamma} < 75 \text{ GeV}/c$				
m_h (GeV/c^2)	ϵA (%)		Event Yields			
	VH	VBF	Signal	Background	Data	S/\sqrt{B}
100	4.04	4.65	41.6	132	137	3.6
105	3.91	4.59	19.7	114	102	1.8
110	3.91	4.66	10.0	87.3	91	1.1
115	3.86	4.67	5.2	75.9	72	0.6
120	3.93	4.81	3.0	80.4	79	0.3
125	3.86	4.81	1.7	67.0	73	0.2
130	3.86	4.87	1.1	55.7	54	0.1
135	3.77	4.85	0.7	47.9	49	0.09
140	3.80	4.95	0.4	49.2	50	0.06
145	3.75	4.93	0.3	43.1	43	0.04
150	3.71	4.95	0.2	35.6	38	0.03

(b)

Fermiophobic $h \rightarrow \gamma\gamma$		CDF Run II Preliminary				
CP Category (9.3 fb^{-1})		$35 < p_T^{\gamma\gamma} < 75 \text{ GeV}/c$				
m_h (GeV/c^2)	ϵA (%)		Event Yields			
	VH	VBF	Signal	Background	Data	S/\sqrt{B}
100	4.76	4.88	44.7	681	706	1.7
105	4.84	4.98	22.1	629	619	0.9
110	4.81	4.94	11.1	552	522	0.5
115	4.74	5.00	5.8	496	470	0.3
120	4.85	5.13	3.3	582	533	0.1
125	4.74	5.19	1.9	520	488	0.08
130	4.68	5.11	1.2	449	408	0.05
135	4.58	5.13	0.7	393	402	0.04
140	4.56	5.22	0.5	422	436	0.02
145	4.52	5.10	0.3	382	377	0.01
150	4.44	5.05	0.2	328	311	0.01

(c)

Fermiophobic $h \rightarrow \gamma\gamma$		CDF Run II Preliminary				
C'C Category (9.9 fb^{-1})		$35 < p_T^{\gamma\gamma} < 75 \text{ GeV}/c$				
m_h (GeV/c^2)	ϵA (%)		Event Yields			
	VH	VBF	Signal	Background	Data	S/\sqrt{B}
100	1.00	1.13	10.1	42.0	42	1.6
105	0.98	1.15	4.9	40.0	30	0.8
110	0.97	1.18	2.5	32.4	24	0.4
115	0.95	1.17	1.3	26.2	25	0.3
120	1.03	1.23	0.8	25.8	36	0.2
125	0.99	1.22	0.4	24.6	27	0.09
130	0.98	1.28	0.3	20.7	20	0.06
135	0.94	1.21	0.2	18.6	15	0.04
140	0.97	1.24	0.1	18.7	16	0.02
145	0.93	1.28	0.07	13.4	19	0.02
150	0.93	1.26	0.04	12.3	13	0.01

(d)

Fermiophobic $h \rightarrow \gamma\gamma$		CDF Run II Preliminary				
C'P Category (9.3 fb^{-1})		$35 < p_T^{\gamma\gamma} < 75 \text{ GeV}/c$				
m_h (GeV/c^2)	ϵA (%)		Event Yields			
	VH	VBF	Signal	Background	Data	S/\sqrt{B}
100	0.52	0.52	4.8	143	129	0.4
105	0.56	0.59	2.6	120	98	0.2
110	0.54	0.56	1.2	89.8	83	0.1
115	0.54	0.58	0.7	72.0	87	0.08
120	0.56	0.60	0.4	76.4	104	0.04
125	0.57	0.59	0.2	76.6	90	0.03
130	0.56	0.63	0.1	71.1	68	0.02
135	0.54	0.60	0.08	63.3	63	0.01
140	0.53	0.61	0.05	71.8	63	0.006
145	0.54	0.64	0.03	65.2	55	0.004
150	0.55	0.61	0.02	53.6	51	0.003

c. $p_T^{\gamma\gamma} < 35 \text{ GeV}/c$ Region

TABLE VI: The $p_T^{\gamma\gamma} < 35 \text{ GeV}/c$ region is shown here. For each h_f mass hypotheses tested in this analysis, the efficiency multiplied by signal acceptance (ϵA) is shown as a percentage of the total number of $h \rightarrow \gamma\gamma$ decays for each production mechanism (VH and VBF). These values, along with the cross sections and branching ratios provided in Table I, are used to obtain the predicted number of SM Higgs boson signal events. Integrated luminosities for each channel are given in Section III and provided in each subtable. The number of background and data events are also given for each mass. The final column in each subtable is the number of signal events divided by the square root of the number of background events (S/\sqrt{B}). The event yields for each mass point are obtained from a signal region centered on the Higgs boson mass hypothesis.

(a)							(b)						
Fermiophobic $h \rightarrow \gamma\gamma$				CDF Run II Preliminary			Fermiophobic $h \rightarrow \gamma\gamma$				CDF Run II Preliminary		
CC Category (10 fb ⁻¹)				$p_T^{\gamma\gamma} < 35 \text{ GeV}/c$			CP Category (9.3 fb ⁻¹)				$p_T^{\gamma\gamma} < 35 \text{ GeV}/c$		
m_h (GeV/ c^2)	ϵA (%)		Event Yields				m_h (GeV/ c^2)	ϵA (%)		Event Yields			
	VH	VBF	Signal	Background	Data	S/\sqrt{B}		VH	VBF	Signal	Background	Data	S/\sqrt{B}
100	2.32	2.68	23.9	679	661	0.9	100	2.89	3.06	27.3	4617	4577	0.4
105	2.19	2.70	11.1	570	550	0.5	105	2.76	3.10	12.9	3804	3825	0.2
110	2.10	2.66	5.4	450	435	0.3	110	2.69	3.02	6.3	3008	3047	0.1
115	2.01	2.63	2.8	379	388	0.1	115	2.59	3.04	3.3	2616	2612	0.06
120	1.99	2.70	1.6	402	432	0.08	120	2.54	3.09	1.8	2853	2838	0.03
125	1.95	2.66	0.9	349	371	0.05	125	2.44	3.05	1.0	2475	2499	0.02
130	1.86	2.68	0.5	285	311	0.03	130	2.34	3.02	0.6	2029	2038	0.01
135	1.84	2.67	0.3	253	272	0.02	135	2.29	2.97	0.4	1791	1773	0.009
140	1.76	2.73	0.2	265	273	0.01	140	2.18	2.99	0.2	1876	1815	0.005
145	1.73	2.74	0.1	236	239	0.009	145	2.10	2.94	0.1	1640	1613	0.004
150	1.65	2.72	0.08	211	182	0.005	150	2.06	2.95	0.09	1369	1356	0.002

(c)							(d)						
Fermiophobic $h \rightarrow \gamma\gamma$				CDF Run II Preliminary			Fermiophobic $h \rightarrow \gamma\gamma$				CDF Run II Preliminary		
C'C Category (9.9 fb ⁻¹)				$p_T^{\gamma\gamma} < 35 \text{ GeV}/c$			C'P Category (9.3 fb ⁻¹)				$p_T^{\gamma\gamma} < 35 \text{ GeV}/c$		
m_h (GeV/ c^2)	ϵA (%)		Event Yields				m_h (GeV/ c^2)	ϵA (%)		Event Yields			
	VH	VBF	Signal	Background	Data	S/\sqrt{B}		VH	VBF	Signal	Background	Data	S/\sqrt{B}
100	0.58	0.71	5.9	233	228	0.4	100	0.33	0.37	3.1	1017	1044	0.1
105	0.58	0.69	2.9	181	194	0.2	105	0.35	0.38	1.6	7167	669	0.06
110	0.53	0.69	1.4	149	120	0.1	110	0.32	0.38	0.8	503	493	0.03
115	0.49	0.65	0.7	115	112	0.06	115	0.30	0.37	0.4	420	442	0.02
120	0.50	0.71	0.4	120	113	0.04	120	0.31	0.38	0.2	440	495	0.01
125	0.50	0.69	0.2	93.3	114	0.02	125	0.32	0.39	0.1	389	433	0.007
130	0.48	0.71	0.1	82.6	78	0.02	130	0.29	0.37	0.07	331	344	0.004
135	0.46	0.70	0.08	69.7	77	0.01	135	0.29	0.37	0.05	298	288	0.003
140	0.47	0.69	0.05	78.7	73	0.006	140	0.28	0.38	0.03	314	300	0.002
145	0.46	0.69	0.03	69.7	65	0.004	145	0.28	0.38	0.02	278	266	0.001
150	0.44	0.70	0.02	61.7	57	0.003	150	0.25	0.36	0.01	235	215	0.001